

Micromachined p-GaN Gate Normally-off Power HEMT with an Optimized Air-bridge Matrix Layout Design

Chih-Wei Yang, , Hsiang-Chun Wang, Hsien-Chin Chiu, Chien-Kai Tung*, Tsung-Cheng Chang*, Schang-jing Hon*

Department of Electronics Engineering, Chang Gung University, Taiwan, R.O.C.

HUGA OPTOTECH Inc. Taichung, Taiwan, R.O.C.*

TEL: +886-3-2118800 # 3645 Email: hcchiu@mail.cgu.edu.tw

Abstract

In this work, a micromachined P-GaN power high electron mobility transistor (HEMT) on Si substrate with new air-bridged matrix design was demonstrated. Fig.1 shows the cross-section of P-GaN HEMT with micromachined. The device with a 2 μm gate length which was on top of 4 μm length P-GaN layer, the gate-to-source and gate-to-drain distance were 6 μm and 20 μm , respectively. After the completion of the front-side fabrication, the Si substrate was thinned down to 100 μm . Then the Si substrate beneath the active region was removed by SF_6 plasma etching, until the N-face buffer layer was exposed. For reducing the substrate leakage current and enhancing the thermal management, the SiO_2/Cu (100 nm/20 μm) were deposited on the backside of the 4 inch wafer. In order to compare the device characteristics, the standard power device with parallel drain/source multi-fingers (MF) design which shown in Fig. 1(c) and 1(d) was fabricated on the same wafer and the device size is 1.34 \times 1.34 mm^2 . Figure 2(a) and 2(b) exhibited the previous design called air-bridge matrix (ABM), and the new ABM design was shown in Fig 2(c) and 2(d). For comparison, size of both devices is 1.34 \times 1.34 mm^2 . Fig. 3 displays $I_{\text{DS}}-V_{\text{GS}}$ and $g_{\text{m}}-V_{\text{GS}}$ characteristics of MF, ABM and new ABM P-GaN HEMT with backside micromachined at $V_{\text{DS}} = 5 \text{ V}$, respectively. An obvious current improving is observed for ABM and new ABM P-GaN HEMT due to the air-bridge matrix structure increases the current density from one-dimension to two-dimensions. As shown in Fig. 3, threshold voltages (V_{th}) of three devices were +0.7 V; the I_{DS} is 1.55 A of MF P-GaN HEMT and it can be improved to 2.28 A by using the new ABM design, it is about 47 % current improving. Fig. 4 presents the $I_{\text{DS}}-V_{\text{DS}}$ characteristic of three HEMTs with backside micromachined at V_{GS} from 4 to 0 V. The $R_{\text{DS,on}}$ was extracted at $V_{\text{GS}} = 4 \text{ V}$; and it is 2.25 Ω for MF P-GaN HEMT, 1.9 Ω for ABM P-GaN HEMT and 1.64 Ω for new ABM P-GaN HEMT, respectively. The smaller $R_{\text{DS,on}}$ for new ABM P-GaN HEMT was ascribed to improve the current density, increase the total gate width and reduce the transmission distance between drain and source region. In addition, the current flow of MF-HEMT is one-dimension, and the current crowding occurs at the drain electrode due to high electric field. However, the current flows of ABM and new ABM design were two-dimension, therefore the current can be distributed and current crowding can be weakened. The three-terminal off-state breakdown voltages (V_{BR}) of three HEMTs measured using an Agilent B1505A measurement system was shown in Fig. 5. In this work, V_{BR} is defined as the voltage at which a drain leakage current between the drain and the source terminals reaches 1 mA at a V_{GS} of 0 V. The drain leakage current of MF P-GaN HEMT increases rapidly following an increase of V_{DS} and its V_{BR} is 188 V. This value can be improved to 274 V with new ABM design due to the mesa sidewall leakage path was eliminated by the air-bridged structure. Fig. 6 shows the dynamic R_{on} measurement which measured by using an Agilent 1267A measurement system. Devices were biased at on-state ($V_{\text{GS}} = 5 \text{ V}$ and $V_{\text{DS}} = 2 \text{ V}$) and off-state ($V_{\text{GS}} = 0 \text{ V}$, $V_{\text{DS}} = 0$ to 110 V). An obvious increase of R_{on} was obtained from MF P-GaN HEMT with an increase of V_{DS} . On the other hand, ABM P-GaN HEMT shows a slighter increase of R_{on} than the new ABM one. It is believed that the drift regions of new ABM design is larger than ABM design and caused higher surface traps and made the higher increase of R_{on} .

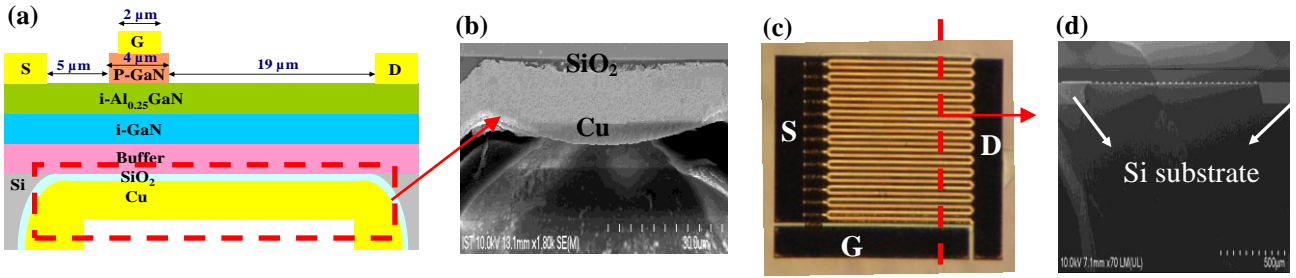


Fig. 1 (a) Cross-section of P-GaN HEMT with backside micromachined. (b) SEM image of backside micromachined. (c) Top-view of multi-finger P-GaN HEMT. (device size = $1.34 \times 1.34 \text{ mm}^2$) (d) SEM image of multi-finger P-GaN HEMT with backside micromachined.

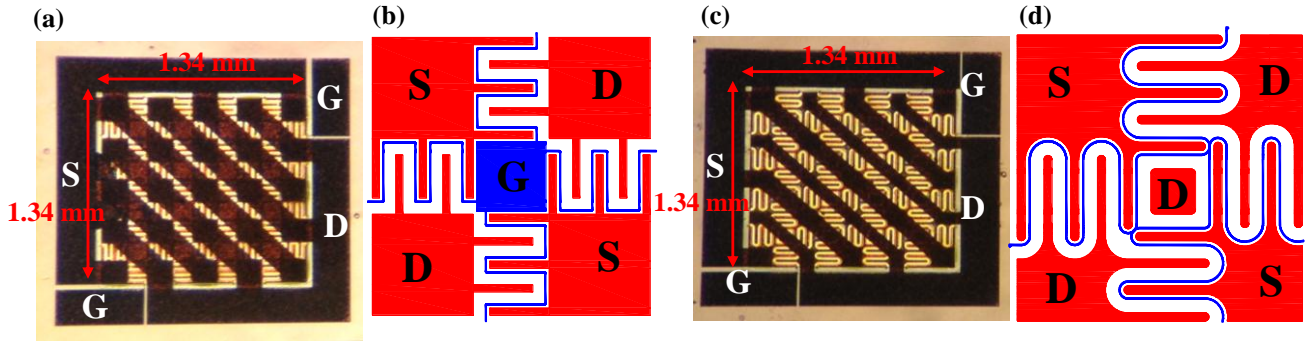


Fig.2(a) Top-view of ABM P-GaN HEMT (device size = $1.34 \times 1.34 \text{ mm}^2$) (b) ABM Layout of a 2×2 matrix cell. (c) Top-view of new ABM P-GaN HEMT. (device size = $1.34 \times 1.34 \text{ mm}^2$) (d) New ABM Layout of a 2×2 matrix cell.

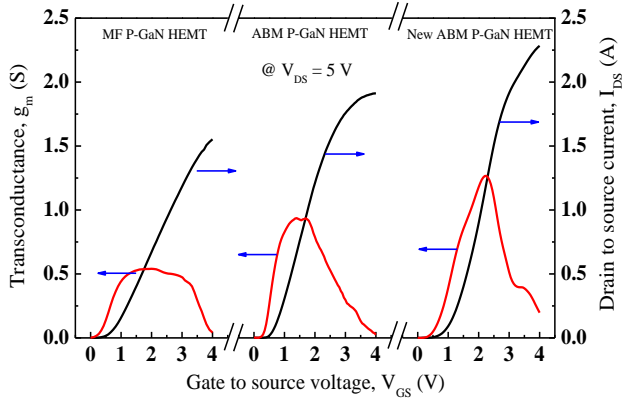


Fig.3 $I_{DS}-V_{GS}$ and g_m-V_{GS} characteristic of MF, ABM and new ABM P-GaN HEMT with backside micromachined at $V_{DS} = 5 \text{ V}$.

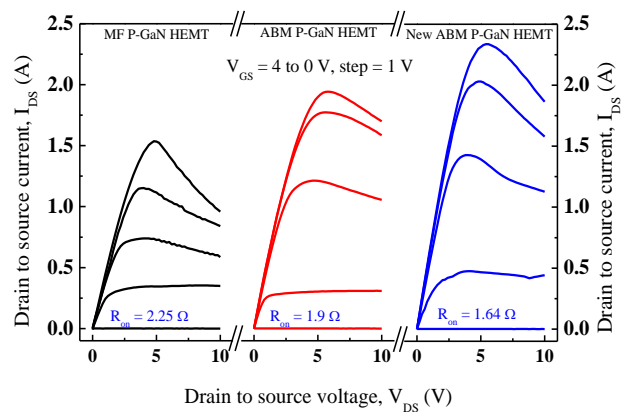


Fig. 4 $I_{DS}-V_{DS}$ characteristics of MF, ABM and new ABM P-GaN HEMT with backside micromachined.

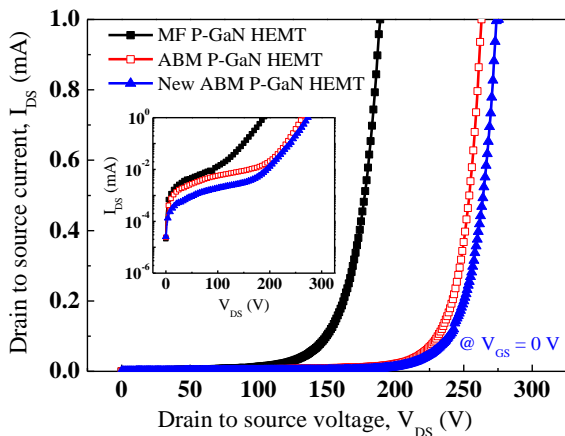


Fig.5 Three-terminal off-state breakdown voltage measurements for MF, ABM and new ABM P-GaN HEMT with backside micromachined at $V_{GS} = 0 \text{ V}$.

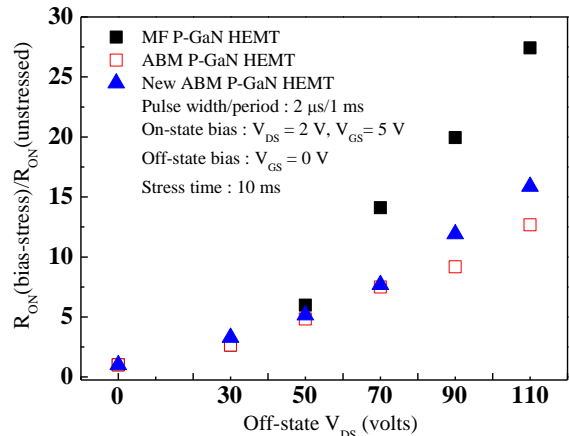


Fig.6 Dynamic R_{on} measurement for MF, ABM and new ABM P-GaN HEMT with backside micromachined.